# A STUDY OF THE EFFECT OF SURFACE FILMS ON FATIGUE FRACTURE

ANNUAL SUMMARY REPORT
15 August 1963 - 14 August 1964

MRI Project No. RA-14-P

Contract Nonr-3908(00)







For

Office of Naval Research
Metallurgy Branch
Materials Science Division
Attn: Code 423 (Dr. W. G. Rauch)

MRI
MIDWEST RESEARCH INSTITUTE

MIDWEST RESEARCH INSTITUTE

# A STUDY OF THE EFFECT OF SURFACE FILMS ON FATIGUE FRACTURE

by

J. C. Grosskreutz
C. Quinton Bowles

ANNUAL SUMMARY REPORT
15 August 1963 - 14 August 1964

MRI Project No. RA-14-P

Contract No. Nonr-3908(00)

For

Office of Naval Research
Metallurgy Branch
Materials Science Division
Attn: Code 423 (Dr. W. G. Rauch)

cs

## PREFACE

This report was prepared by the Mathematics and Physics Division of Midwest Research Institute, Kansas City, Missouri, and covers the research performed during the period 15 August 1963 - 14 August 1964 under Contract Nonr-3908(00). The work was directed by Dr. J. C. Grosskreutz under the supervision of Dr. Sheldon L. Levy, Director, Mathematics and Physics Division. Others contributors to this project were Mr. C. Quinton Bowles, Assistant Physicist and Mr. G. Gordon Shaw, Senior Electron Microscopist.

Approved for:

MIDWEST RESEARCH INSTITUTE

S L Levy

Sheldon L. Levy, Director
Mathematics and Physics Division

18 September 1964

## TABLE OF CONTENTS



## List of Tables

TABLE OF CONTENTS (Continued)

List of Figures

TABLE OF CONTENTS (Concluded)

List of Figures (Concluded)

# I. INTRODUCTION

This report summarizes the second year of effort which has been devoted to a study of dislocation-surface interactions. The present work has as its main objective the observation of the motion and configuration of dislocations near the surface of materials and of the effect of surface films on these parameters. The philosophy and general approach to the problem were discussed in the First Annual Summary Report[1] and will not be repeated here.

Work during the past year has concentrated in four areas: (1) certain modifications and refinements in the ultra-high vacuum (UHV) cyclic straining device, (2) experimental investigation of polycrystalline aluminum with natural oxide layers, (3) investigation of single crystal aluminum under four different anodic layer thicknesses, and (4) investigation of polycrystalline gold whose surface is oxide-free. At the present time, the single crystal aluminum studies are still in progress; but sufficient data have been collected at the low strain amplitudes so that conclusions consistent with the polycrystalline aluminum and gold work can be drawn. This report discusses each of the above areas in turn and then proceeds with a general discussion of the results.

A paper describing our work on the structure of anodic layers on aluminum, which was performed during the first year's effort, appeared in the July 1964 issue of Journal of Applied Physics, p. 2195. A paper entitled "A New Method of Disk Electropolishing for Transmission Electron Microscopy using Polystyrene Masks," by G. Gordon Shaw and C. Quinton Bowles will be presented at the 1964 meeting of the Electron Microscope Society of America to be held in Detroit, October 13 - 17. Another paper entitled "Dislocation Induced Surface Strains in Deformed Aluminum and Gold" is under preparation and will be submitted for publication.

# II. REFINEMENTS IN ULTRA-HIGH VACUUM CYCLIC STRAINING DEVICE

Provision has been made for accurate measurement of the absolute pressure in the test chamber, and means are now available for measuring the strain hardening which occurs during cyclic bending.

## A. Vacuum Measurement

A Varian type UHV-12-K ionization gage was purchased and installed to read the pressure in the vicinity of the test sample. These gages are accurate down to the $10^{-11}$ Torr range. With our present chamber, we consistently reach vacua of $1.3 \times 10^{-9}$ Torr with the sample in place.

B. Cyclic Strain Hardening Measurements

To obtain the cyclic strain hardening curve, we decided simply to measure the force required during each half cycle to produce the desired strain amplitude. To obtain maximum sensitivity and to reduce to a minimum all extraneous forces, it was decided to make the measurements inside the vacuum chamber. Silicon p-doped semiconductor strain gages with a gage factor of approximately 120 were obtained from Microsystems, Inc. One of these was mounted on each side of one of the leaf springs as shown in Fig. 1.* By connecting these gages in series, the total signal was increased by a factor of two.

Using a Videc Instruments Co. pre-amplifier and a Brush Mk. II two-channel recorder, we obtained a sensitivity of 0.25 lb. in each half cycle. It is necessary, however, to ultimately withstand a 300°C vacuum bakeout and the $1.3 \times 10^{-9}$ vacuum. So far we have not been successful in our efforts.

At present we have on order from Baldwin-Lima-Hamilton some similar gages with platinum lead wires bonded in a somewhat different manner. These, along with the W. T. Bean type "H" high temperature cement which we have already tested, should produce satisfactory results under all expected conditions including the bakeout.

## III. DESIGN OF EXPERIMENTS

The general experimental arrangement including sample size, shape and mode of deformation has already been described.[1] In this section, we are concerned with the choice of experimental variables and their magnitudes, as well as the observables which are recorded during the experiment.

Seven experimental variables were considered: temperature, cyclic frequency, number of strain cycles, strain amplitude, crystal orientation, oxide layer thickness and environmental pressure. For consideration of fatigue crack initiation, the early cycling period is most important; therefore, we limit ourselves to the initial rapid hardening state. For the work on aluminum, the following choices of parameters were made:

1. Number of strain cycles - up to four different cycle levels in the rapid hardening state.

---

* All figures appear in the Appendix, p. 15.

2. Oxide layer thickness - natural oxide (40 Å), 100 Å, 300 Å, and 1,000 Å.

3. Surface amplitude - $6 \times 10^{-4}$; $1.5 \times 10^{-3}$.

4. Crystal orientation - polycrystals; single crystals oriented for single slip (crystal face, {210} ).

5. Environmental pressure - atmospheric (760 Torr); $1 \times 10^{-9}$ Torr.

6. Temperature - room temperature.

7. Frequency - 2 cycles/sec.

Parameters chosen for observation are the following:

1. Disposition and height of surface slip steps.

2. Near surface dislocation configuration.

3. Surface hardness.

## IV. EXPERIMENTAL RESULTS

### A. Polycrystalline Aluminum

These experiments were the first to be carried out in our UHV chamber and do not encompass as wide a variation in experimental conditions as do the single crystal experiments to be described later. Means for measuring the cyclic hardening had not yet been installed at the time of these runs. Two samples were run for 5,000 cycles in a vacuum of $4 \times 10^{-9}$ Torr and at strain levels of $5.2 \times 10^{-4}$ and $1.3 \times 10^{-3}$, respectively. (These figures refer to surface strains in bending.) Two additional samples were run at 760 Torr using the above same parameters. The other experimental conditions were as indicated in Section III above.

Method of sample preparation: Pieces 3 in. x 1 in. x 5/16 in. were sawed from 99.99 per cent pure aluminum billets and rolled in a hand rolling mill to an average thickness of 0.50 in. At this point, they were annealed for 3 hr. at 350°C and pressed under a hydraulic ram to produce smooth surfaces. All samples were then machined in a stack in a milling machine to give the required sample configuration. Electropolishing was carried out in the usual perchloric acid - ethyl alcohol mixture at 10 - 15°C for about 30 min. with a final polish in a nitric acid-methyl alcohol mixture at -25°C for 5 - 8 min. The resulting surface was free of any hillock structure within the resolution of our electron microscope.

In order that all samples could have the same final heat treatment, two samples were placed in the bottom of the vacuum chamber on microscope slides and the other two were mounted in the cycling fixture. After reaching a vacuum of $\sim 2 \times 10^{-6}$ Torr, the bakeout was started. This produced a very slow anneal lasting about 24 hr. with 6 hr. at 350°C in a vacuum which did not rise above $5 \times 10^{-5}$ Torr. This heat treatment produced a fairly uniform grain size having an average cross section of 250 - 300 microns.

Surface slip patterns: Optical micrographs of surfaces of the four samples are given in Figs. 2 and 3. A statistical analysis made of the slip patterns in the various grains showed that at the high strain amplitude the surface slip distribution was essentially the same at 760 Torr and at $4 \times 10^{-9}$ Torr. At low-strain amplitude, however, significantly fewer slip bands were found on the surface of the sample strained in high vacuum. Electron micrographs of surface replicas were taken of the low-strain samples and typical results are shown in Fig. 4. The distinguishing feature is that practically every grain of the sample cycled in UHV was covered with fine slip while the samples cycled in air tended to have slip concentrated into bands with no observable slip between the bands. In all cases of fine slip, the spacing was of the order of 700 Å. The average slip height in the vacuum runs was 50 - 100 Å while at atmospheric pressure the slip height ranged from 90 - 300 Å.

Near surface dislocation arrangement: The slipped surface of the samples was protected with "microstop" and electropolished from the opposite side until perforation occurred. The details of this technique, especially developed on this project, will be presented in a forthcoming paper.[2] Such foils when viewed in transmission in the electron microscope reveal the dislocation arrangement just beneath the surface of interest.

Two general observations were made. The first is illustrated in Fig. 5 which shows a high density of dislocation loops and tangles together with a faint outline of the surface slip-line structure in the lower right-hand corner of the topmost grain in the figure. The dislocation tangles do not seem to bear any relation to the slip-line structure, while the dislocation loops appear to have some tendency to line up in the direction of the slip lines. The second, and quite frequent observation in the UHV samples, was the appearance of slip-line structure as shown in Fig. 6. Numerous dislocation loops and line fragments can be seen associated with these slip-line patterns.

The slip shown in Fig. 6 is visible by diffraction contrast; that is, the sample must be tilted to the proper Bragg angle to bring the slip into view. Confirmation of this fact is shown in Fig. 7(b) in which the slip lines are shown in strong contrast near an extinction contour. Fig. 7(a), shown for comparison, is a surface replica which confirms the slip-line spacing.

Similar contrast can also be observed in foils prepared from samples cycled at 760 Torr, but on a less extensive scale. In either case, the contrast is bleached out rapidly by contamination under the electron beam. Photographic exposures were therefore made with the least practical beam intensity.

Origin of diffraction contrast at slip lines: The observed contrast has two possible origins. It may arise as a dynamical interference due to the thickness variation caused by the slip steps, or it can be due to lattice strains remaining in the vicinity of the slip planes. The operating reflection in Fig. 7(b) is (200) for which the extinction distance is 774 Å. The slip-line height is $\sim$100 Å, so that the contrast arising from a simple thickness variation would not be too strong. There exist, however, better criteria, based on the dynamical theory of diffraction contrast,[3] for deciding between the two possible origins of the contrast, and these are discussed below.

First, dynamical interference due to thickness variation should become weaker in thicker regions of the foil on account of absorption effects. Strain contrast should be little affected by thickness, except perhaps in the thinnest portions where strain relief should occur. Second, a comparison of bright and dark field images taken with the foil oriented so that the slip is first on top and then on the bottom can be most instructive. For thicknesses of the order of four extinction distances or greater, absorption effects will be such that images arising from strain contrast will be complementary only for slip on the bottom of the foil, provided the strains are, indeed, located at the slipped surface. For thickness variation contrast, the images will be complementary in bright and dark fields regardless of foil orientation.

Experiments were performed to test each of the above criteria and, in every case, it was clear that the observed contrast is due to surface strains associated with the slip lines. A more detailed account of these experiments will be given in a paper now in preparation.

## B. Single Crystal Aluminum

To date, crystals of aluminum oriented for a single slip have been cycled at low strain, $6 \times 10^{-4}$, both in vacuum ($1.3 \times 10^{-9}$ Torr) and at atmospheric pressure. A complete study along the lines discussed in Section III has been carried out on these crystals.

Method of sample preparation: Aluminum single crystals of 99.99 per cent purity and oriented for single slip were purchased from Semi-Elements, Inc., as blanks 5-3/4 in. x 2-3/8 in. x 1/16 in. These were hand-lapped on glass plates using No. 240, No. 400 and No. 600 grit silicon carbide grinding powder.

At this point, they were treated with sodium hydroxide solution and electropolished in the usual perchloric acid-ethyl alcohol mixture at 10 - 15°C for about 20 min. The final sample shape was obtained using a special tool in a "Servo-met" spark machining unit. A final polish of 15 min. in the perchloric acid-ethyl alchohol mixture and 5 - 8 min. in the nitric acid-methyl alcohol mixture produced the final surface finish.

Four different anodic layers consisting of natural oxide, 100 Å, 300 Å, 1,000 Å, were put on each sample, the last three using the technique developed by Grosskreutz and Shaw.[4]

The samples were finally placed in the vacuum chamber for annealing as described in the section for preparing polycrystalline samples.

Hardening measurements: The cyclic hardening of the sample deformed at atmospheric pressure was found to be negligible throughout 5,000 cycles of strain. This finding is consistent with the results of Snowden[5] who found that crystals oriented for single slip hardened very slowly at low-strain amplitudes.

Surface hardness measurements were made under each of the four different anodic layer thicknesses of both the sample deformed at atmospheric pressure and the sample deformed at $1.3 \times 10^{-9}$ Torr using a diamond microindentor. The anodic layers were removed in 2 per cent hydrofluoric acid solution prior to measurement. Table I gives the measured hardnesses of these samples as well as a control (uncycled sample subjected to the same heat treatment). The sample was slightly harder under the thicker oxide coatings.

TABLE I

VICKERS HARDNESS NUMBERS FOR SAMPLES DEFORMED 5,000 CYCLES AT $6 \times 10^{-4}$ STRAIN AS WELL AS CONTROL SAMPLE

(Average of Six Points)

| Sample | Vickers Numbers According to Oxide Thickness | | | |
|---|---|---|---|---|
| | Nat. Oxide | 100 Å | 300 Å | 1,000 Å |
| Crystal run at 760 Torr | 14.8 | 12.4 | 15.3 | 18.7 |
| Crystal run at $1.3 \times 10^{-9}$ Torr | 16.3 | 13.6 | 15.9 | 17.8 |
| Control Sample | 17.3 | | | |

Surface slip distribution: Optical micrographs of the surfaces of these crystals are shown in Figs. 8 and 9. (No slip was visible at this magnification on the surface of the 300 and 1,000 Å anodic layer coatings.) It should be noted first that there is no significant difference between the slip patterns which appear on the natural and on the 100 Å oxide layers especially in the case of the sample cycled in air. Second, there are striking differences between the surfaces cycled in air and in UHV. As in the polycrystalline case, slip bands do not readily form under UHV. Rather, the slip appears to disperse over the whole surface of the sample.

An extensive series of surface replicas were taken for examination in the electron microscope. The following replicas were prepared.

1. Formvar replicas of the outer anodic layer surfaces.

2. Direct replicas of the anodic layer surface adjacent to the metal.

3. Direct replicas of the underlying metal surface. The oxide was first removed in a solution of $CrO_3$ and $H_3PO_4$ held at 70°C. The onset of pitting of the aluminum surface was used as the criterion for complete removal of the oxide.

The results can be stated briefly for the sample cycled at atmospheric pressure. The top surface of the anodic layers showed evidence of slip in all cases except the 1,000 Å layer. Examples are shown in Fig. 10. The fine slip within the broad slip bands observed on the natural oxide layer (Fig. 10(a)) was not observed on the two heavier anodic layers. The anodic layer surface at the oxide-metal interface showed no evidence of slip for either the 300 Å or 1,000 Å layer. It was not possible to replicate this surface in the case of the 100 Å or natural oxide layer. Direct replicas of the metal surface showed slip under both the 100 Å layer and the 300 Å layer. Some questionable examples of slip were found under the 1,000 Å layer. Representative micrographs are shown in Fig. 11. The resolution in these latter pictures leaves much to be desired, mainly because of the attack of the solution used to remove the anodic layers.

Electron micrographs of replicas taken from the sample deformed in vacuum seem to substantiate the pattern of dispersed slip observed in the optical photographs.

Figures 12 and 13 are a series of micrographs of the top of the anodic layers. Although the slip on the natural oxide layer appears rather heavy, the general pattern extended over more than one field of view in almost every case. The extremely fine slip exhibited on the 100 Å layer appeared on about 60 per cent of the replica and presented itself as broad patches with a slip-line height of ~50 Å. The phenomenon of the slipped surface appearing very smooth and the unslipped surface appearing very rough, as seen on the 100 Å layer, was observed over the entire sample.

Neither the 300 Å or 1,000 Å oxide layers exhibited a definite slip-line pattern; however, the smooth area-rough area parallel appeared on every replica and suggests that these smooth patches would have developed slip patterns had the deformation been more severe.

After removing the oxide and replicating directly the metal surface, a definite slip pattern appeared under the 300 Å layer as shown in Figs. 14(a) and 14(b). The 1,000 Å layer still showed no slip lines; however, the smooth area-rough area pattern prevailed indicating that it is not just a rumpling of the oxide layer. It is interesting to note that in Figs. 14(b) and 14(c) the shadowing angle of 14° presents a particle height of 200 - 300 Å and 700 - 1,000 Å, respectively, indicating that they might be remaining oxide particles.

Near surface dislocation arrangements: Thinning of foils taken from the two single crystals discussed above has only just begun at the time of writing this report.

## C. Polycrystalline Gold

As one of the noble metals, gold does not form an oxide layer on its surface, although reports can be found in the literature which state that very thin layers of adsorbed oxygen do exist.[6] Gold, therefore, offers the opportunity for observing dislocation-surface interactions at an essentially free surface. Investigation of such a material is necessary for the proper interpretation of the slip-line contrast observed in the transmission photographs shown in Figs. 6 and 7. Discussion of this important point is given in more detail below.

Method of sample preparation: Rolled, polycrystalline gold sheet, (99.9+ per cent) 0.005 in. thick was obtained for this experiment. The surface of the gold was electropolished after the method of Westdrop et al.[7] The polishing rates required to produce a smooth surface are such that approximately one day per sample was needed in the polishing bath.

Because deformation under conditions of ultra-high vacuum is unnecessary, these specimens were cycled after the method described by Grosskreutz and Waldow.[8] With this method, thin foils are cemented to a thick plastic substrate which is in turn cycled in reverse bending. The thin foil essentially is deformed in pure push-pull at constant strain amplitude. Samples were cycled for 5,000 cycles and for 10,000 cycles at a strain amplitude of 0.002. This amplitude was necessary to produce surface slip of approximately the same intensity as that observed in the polycrystalline aluminum (see Section IV-A).

Surface slip distribution: Excellent Formvar replicas of the surface were obtained and a representative micrograph is shown in Fig. 15. Examples of both well dispersed fine-slip (Fig. 15(a)) and concentrated-slip bands were observed. The well dispersed slip was by far the more common of the two. The average slip-line separation was 400 Å.

Near surface dislocation distribution: Samples were thinned from one side using the technique previously described.[2] An electropolishing bath containing 50 per cent hydrochloric acid and 50 per cent orthophosphoric acid was found to be suitable.[9]

As in the case of aluminum, extreme care was taken in photographing these foils in the electron microscope so that contamination would not obscure the details of interest. Fresh foils were placed in the microscope immediately following thinning and exposures were made under very low beam intensities. More often than not, the operator could not distinguish visually the type of detail he was photographing at the time. Following development, the photographs were screened for items of interest. It was also the practice to scan some foils under higher beam intensities so that visual observation could be achieved, and the effects of tilting the foil determined. The effects of contamination and loss of resolution could also easily be followed.

The most important observation was that fine slip lines were imaged by diffraction contrast just as in the case of aluminum. Figure 16(a) illustrates this point very well. Notice also that the images shift position laterally as they cross the extinction contour in the upper right-hand corner. Such behavior is common for images produced by lattice strains. In addition to this type of contrast effect, slip lines in heavily slipped areas were visible by a thickness variation contrast, especially in the thinner portions of the foil. An example is shown in Fig. 16(b).

In the regions of more intense slip, dislocations and dislocation loops could be seen associated with the slip lines. In Fig. 16(b) the correlation is not too clear, but Fig. 17 shows rows of mostly unresolved loops lying along the slip lines.

## V. DISCUSSION OF RESULTS

It would be premature at this stage of our effort to give a complete discussion of the results which we have presented; however, certain results appear to be well enough established to merit closer scrutiny. These include the effect of environment on surface slip, the effect of surface layers in suppressing slip, and the fact that near-surface strains occur at slip-line sites.

It is clear from a comparison of the surface slip distribution in both the polycrystalline and single crystal aluminum samples that the removal of atmospheric gases, so that oxidation cannot occur, results in the suppression of slip-band formation. To gain a clearer understanding of this result, we consider what is already known concerning slip-band development in atmospheric environment. It has been well documented[10] that the initial yielding of aluminum in stage I tensile deformation is accompanied by the formation of extensive fine slip at the surface. As the deformation increases, slip is then concentrated into more or less evenly spaced slip bands for reasons which are still not clear. Apparently, initial yielding is caused by the activation of rather uniformly spaced dislocation sources near the surface. Now, under UHV conditions it may be possible for these sources to continue to operate since they would not be pinned by the oxidation process at surface slip steps. Hence, large areas of fine slip could build up under low cyclic strains as we have observed (see Fig. 4).

This conclusion is further substantiated by the surface replica results for gold (see Fig. 15) cycled in air, in which large areas of fine slip are observed with only an occasional slip band. The fact that gold does not oxidize would permit the continued buildup of fine, well dispersed slip. It might be argued that such behavior is due to a much lower stacking fault energy in gold; but copper, which has a stacking fault energy quite near to gold is known to form extensive slip bands in air.

This dispersal of slip has great significance for the formation of fatigue cracks at a surface. Clearly, such dispersal will postpone the formation of deep intrusions and, hence, lengthen the period of crack nucleation.

We have shown that layers of increasing thickness suppress with increasing effectiveness the slip which occurs on the top surface of the anodic layer. Some evidence of slip, however, is found at the metal-oxide interface even under the thickest anodic layer. With a coherent anodic layer of the type used in this experiment, the effect of the layer is unchanged when the atmospheric pressure is removed. The somewhat larger surface hardness measured

under the thicker anodic layer is presumably due to the pileup of dislocations immediately below the layer. Of great significance to the analysis of these layer effects will be the near-surface transmission electron micrographs which show the dislocation configuration beneath the anodic layer. Since the sample was everywhere subjected to the same strain regardless of the thickness of anodic layer, dislocation densities should be comparable under all layers regardless of thickness. We should expect that it is only the dislocation motion in a thin surface layer which is affected by the presence of the anodic layer.

In both gold and aluminum, dislocation loops are found to be associated with slip lines in regions of intense slip. The greater densities observed in gold are due both to the higher strain level and the fact that the activation energy for climb (by which loops are annihilated) is greater in gold. Presumably, many of the loops initially formed in the slip lines of aluminum have disappeared by climb or by prismatic glide out of the surface. In gold, which has a lower stacking fault energy than aluminum, many single dislocations were observed on glide planes associated with individual slip lines. This was seldom the case in aluminum where the high stacking fault energy makes cross slip easy and the formation of tangles much more probable. These tangles do not seem to associate themselves with any particular slip system.

Perhaps the most interesting point in connection with the near-surface micrographs is the existence of large surface strains in the vicinity of the slip lines, which render these lines visible by diffraction contrast in both polycrystalline aluminum and gold. If this contrast were observable only in aluminum, one might argue that it was due to dislocations piled up under the oxide layer which is always present. The fact that one sees it also in gold forces one to the conclusion that there are surface lattice strains associated with the formation of slip lines. One possible explanation of this phenomenon is given in Fig. 18 which shows the atomic lattice configuration at a slip step one Burger's vector in height. The planes which are responsible for diffraction contrast are shown to be warped in the vicinity of the slip step which would give rise to a contrast of the nature of the one observed. Such strains undoubtedly have an influence on the passage of subsequent dislocations and may account for the "saturation" of surface slip step heights after a given number of cycles. It is well known that if the surface layer is removed by electropolishing, these slip-step heights immediately build up and saturate once again. The resolution of adjacent striations, which are $\sim 700$ Å apart in foils typically $\sim 5{,}000$ Å thick, indicates that the surface strains do not penetrate very far into the foil. These strain images are of the order of 400 Å wide in foils for which the glide plane is oriented at $\sim 45°$ to the surface. Thus, the penetration cannot be greater than 400 Å and is probably much less.

## VI. CONCLUSIONS

The conclusions which can safely be drawn at this stage of our research are listed as follows:

1. The complete absence of a corrosive atmosphere during the deformation of aluminum leads to a postponement of the formation of slip bands in which fatigue cracks are known to initiate. This phenomenon can be explained on the basis of a lack of dislocation pinning at the surface due to oxidation processes.

2. Surface anodic layers suppress surface slip in proportion to their thickness. Although slip may not be observed on the top of thick anodic layers, some slip can still occur at the metal-oxide interface. The amorphous nature of the anodic layer evidently prevents transmission of this step through a thick coating.

3. Debris in the nature of dislocation loops is associated with surface slip lines, the debris being of higher density in gold than in aluminum. The difference is presumably due to a lower activation energy for climb in aluminum.

4. The formation of the slip step results in a lattice strain surrounding the step. This strain occurs regardless of the presence of an oxide layer. This strain may be the cause of slip-step height saturation.

## VII. FUTURE WORK

Our plans for the future call for a completion of the work on aluminum single crystals. The transmission microscopy of near-surface dislocation arrangements will be completed for the samples deformed at the low-strain level. Additional runs will be made at the higher strain level, $1.5 \times 10^{-3}$, for the purpose of ascertaining the effects of anodic layers and environmental pressure on the formation of slip bands. This investigation should be essentially complete at the end of the next quarter of work.

Additionally, our plans call for the investigation of the interaction between loading rate and environmental pressure on the surface deformation of aluminum. The dependence of slip-band width, depth, and spacing on the partial

pressure of oxygen at a constant cycling frequency and temperature will be determined. Then the oxygen pressure will be held constant and the frequency of cycling will be varied and the results noted. From these experiments, we shall try to describe the results using a simple kinetic theory of gas adsorption. In this experiment the strain level, the number of strain cycles, and the oxide layer thickness will be held constant.

Finally, a material of low stacking fault energy, most probably stainless steel, which also forms a surface oxide layer will be examined to determine the surface and near surface deformation characteristics in comparison with the extended results with aluminum. From this experiment, we hope to find the major differences between surface deformation in high and low stacking fault energy materials.

## REFERENCES


1. Annual Summary Report, 20 September 1963, A Study of the Effects of Surface Films on Fatigue Fracture, by J. C. Grosskreutz.

2. Shaw, G. G., and C. Q. Bowles, To be presented at the 1964 meeting of the Electron Microscope Society in Detroit, Michigan, and planned for subsequent publication.

3. Howie, A., and M. J. Whelan, Proc. Roy. Soc., A267, 206 (1962).

4. Grosskreutz, J. C., and G. G. Shaw, J. Appl. Phys., 35, 2195 (1964).

5. Snowden, K. U., Acta Metallurgica, 11, 675 (1963).

6. Hackerman, N., J. Appl. Phys., 22, 1395 (1951).

7. Westdrop, W., H. Kimura, and R. Maddin, Acta Metallurgica, 12, 495 (1964).

8. Grosskreutz, J. C., and P. Waldow, Acta Metallurgica, 11, 717 (1963).

9. Thomas, Kenneth, Private Communication (1964).

10. Wilsdorf, H., and D. Kuhlmann - Wilsdorf, Z. für Angen. Phys., 4, 361, 409, 418 (1952).

Seeger, A., J. Diehl, S. Mader, and R. Rebstock, Phil. Mag., 2, 323 (1959).

## APPENDIX

FIGURES 1 - 18

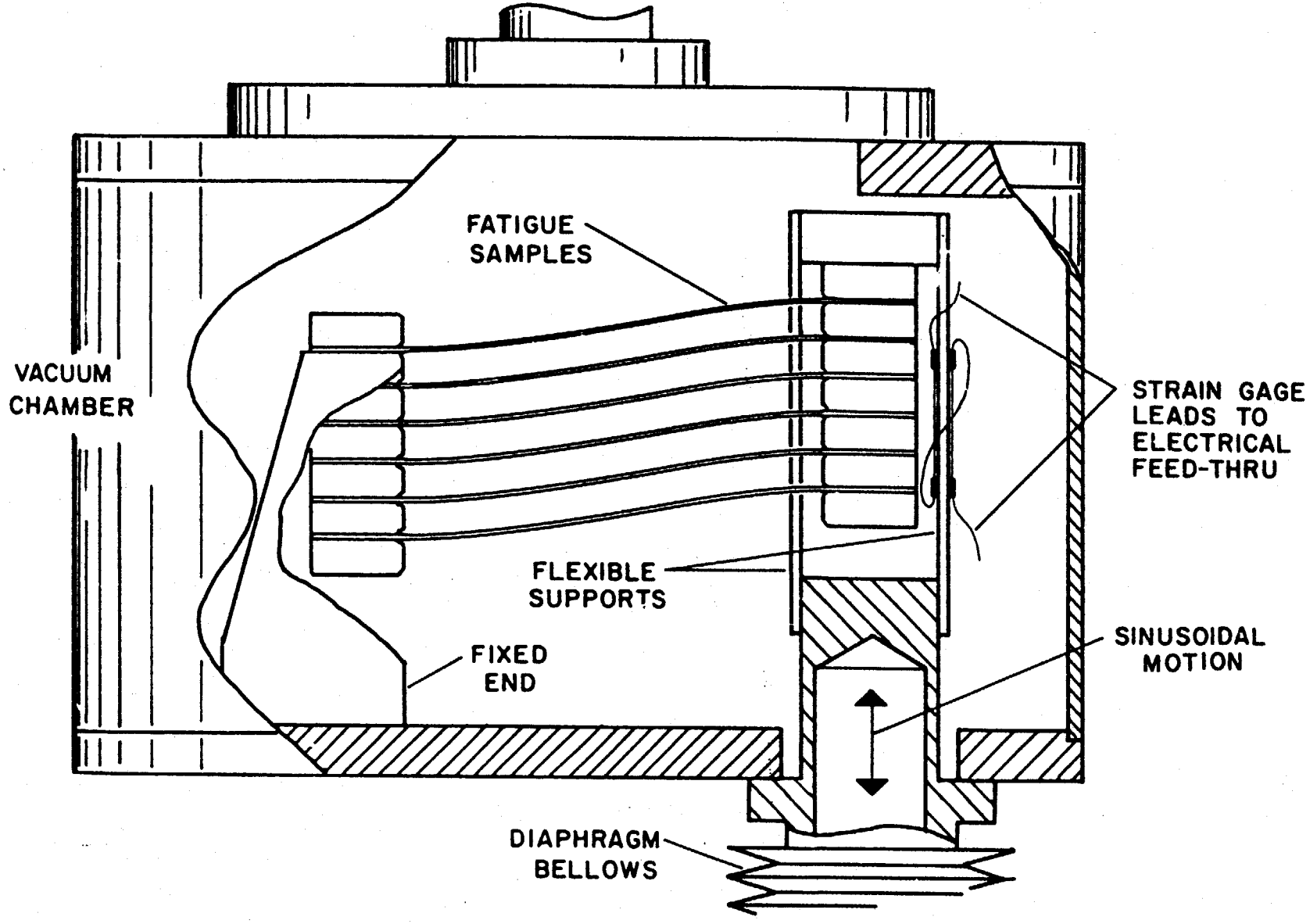


Fig. 1 - Schematic Diagram of Sample Holder in UHV Chamber Including the Mounting of Strain Gages for Strain Hardening Measurements

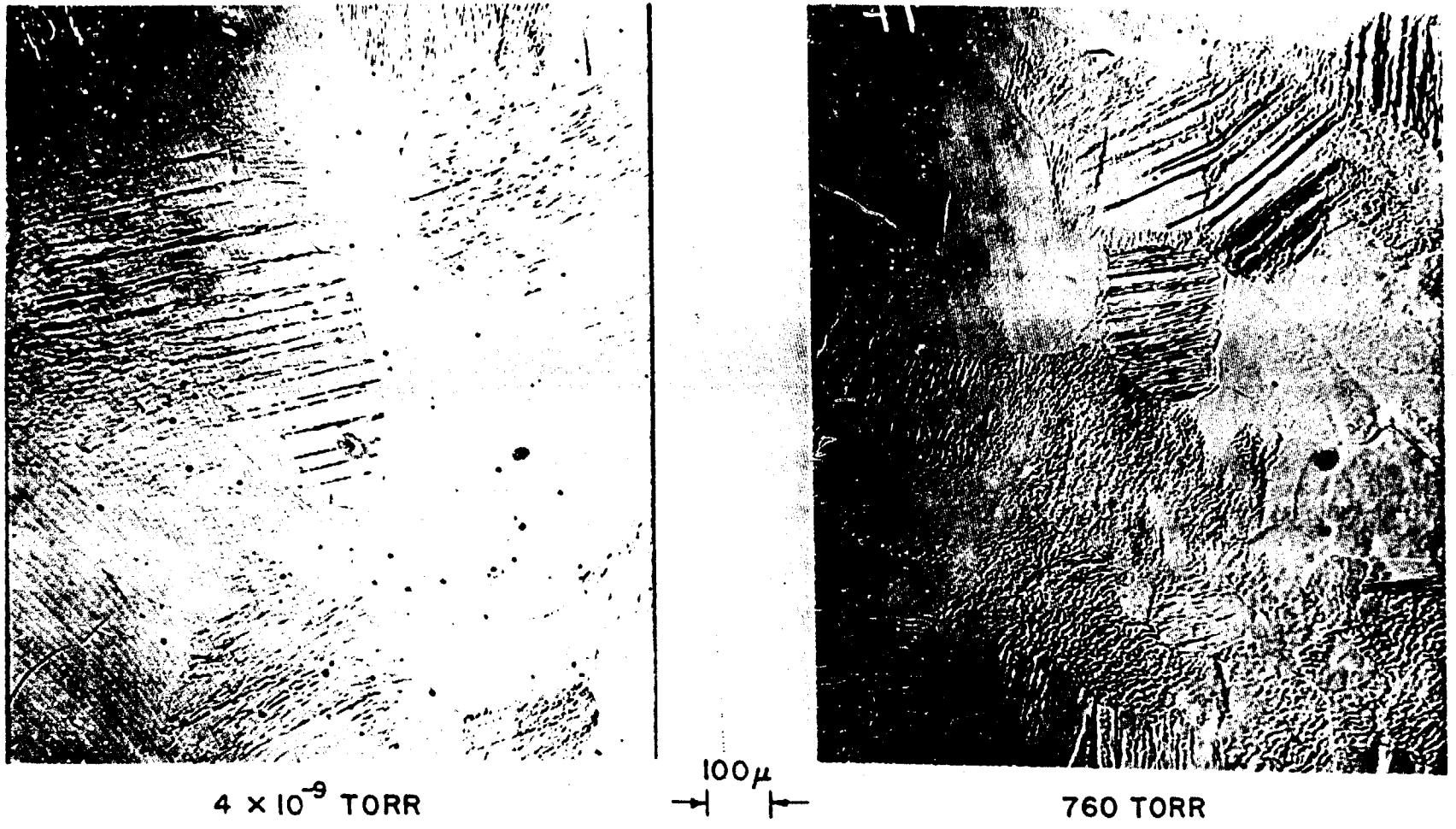


Fig. 2 - Optical Micrographs of Low-Strain Polycrystalline Aluminum Deformed 5,000 Cycles at $\pm$ 5.2 x $10^{-4}$ Strain


Fig. 3 - Optical Micrographs of Low-Strain Polycrystalline Aluminum Deformed 5,000 Cycles at $\pm$ 1.3 x $10^{-3}$ Strain

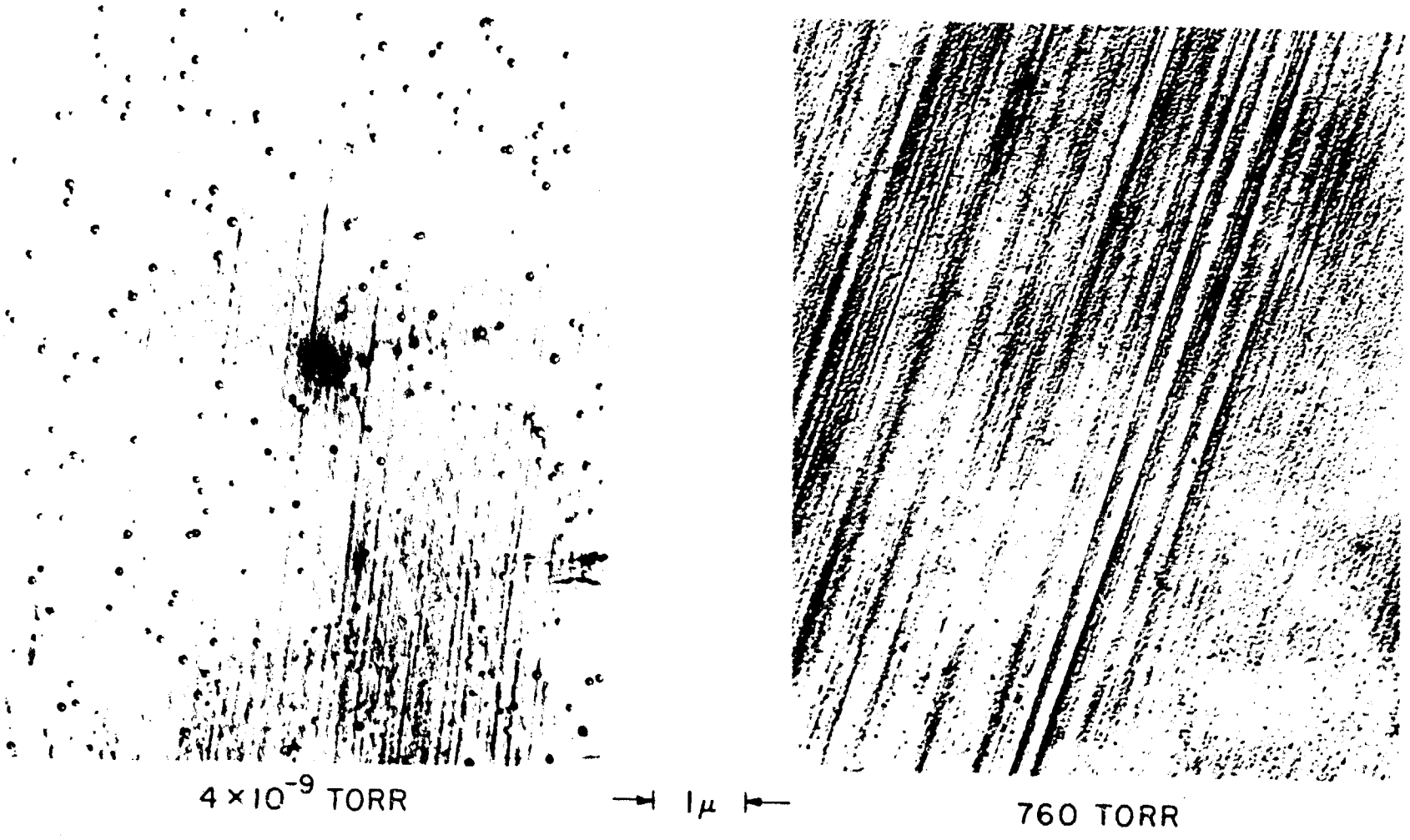


Fig. 4 - Surface Replicas of Polycrystalline Aluminum Deformed 5,000 Cycles at $\pm$ 5.2 x $10^{-4}$ Strain (Shadowing was Pt-Pd at an angle of 14°.)

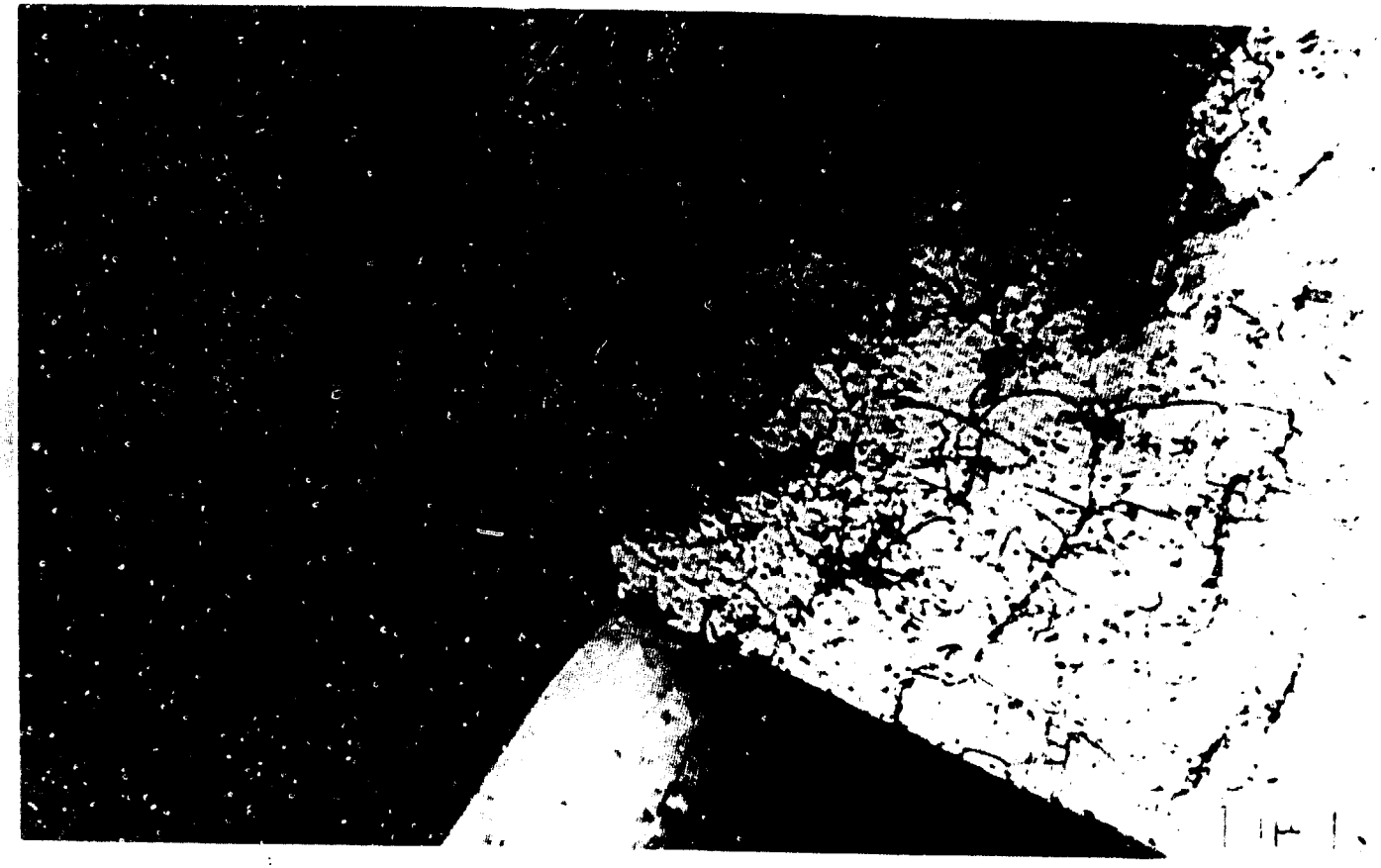

Fig. 5 - Transmission Electron Micrograph of Polycrystalline Aluminum Deformed 5,000 Cycles. Dislocation Loops and Tangles Are Visible over a Background of Fine Slip Lines.

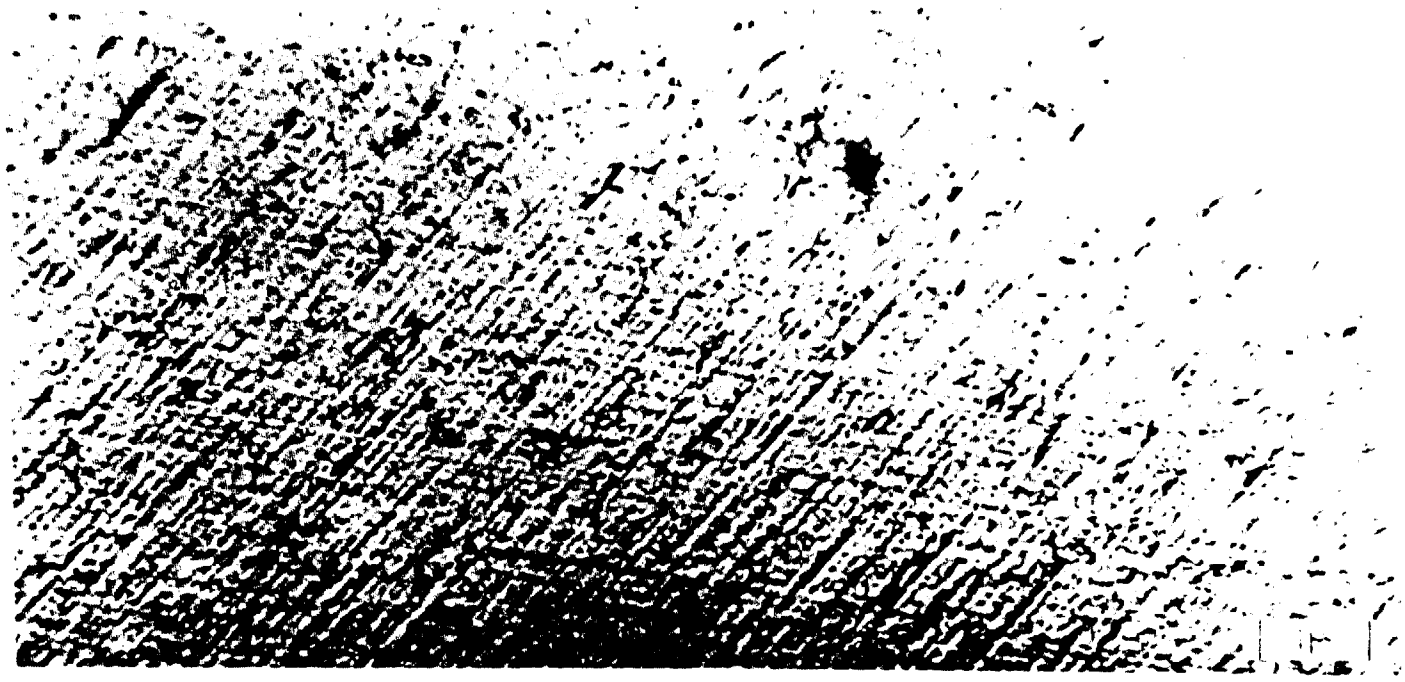

Fig. 6 - Transmission Electron Micrograph of Polycrystalline Aluminum Deformed 5,000 Cycles. Well Ordered Dislocation Loops and Line Fragments Are Visible over the Surface Cross-Slip Pattern.


Fig. 7(a) - Surface Replica (Bradley Shadow, 14°) of Polycrystalline Aluminum Deformed 5,000 Cycles at $\pm$ 5.2 x $10^{-4}$ Strain. Ambient Pressure, 4 x $10^{-9}$ Torr. (Spherical Objects are an Artifact of Preparation Which Show Direction of Shadow.)

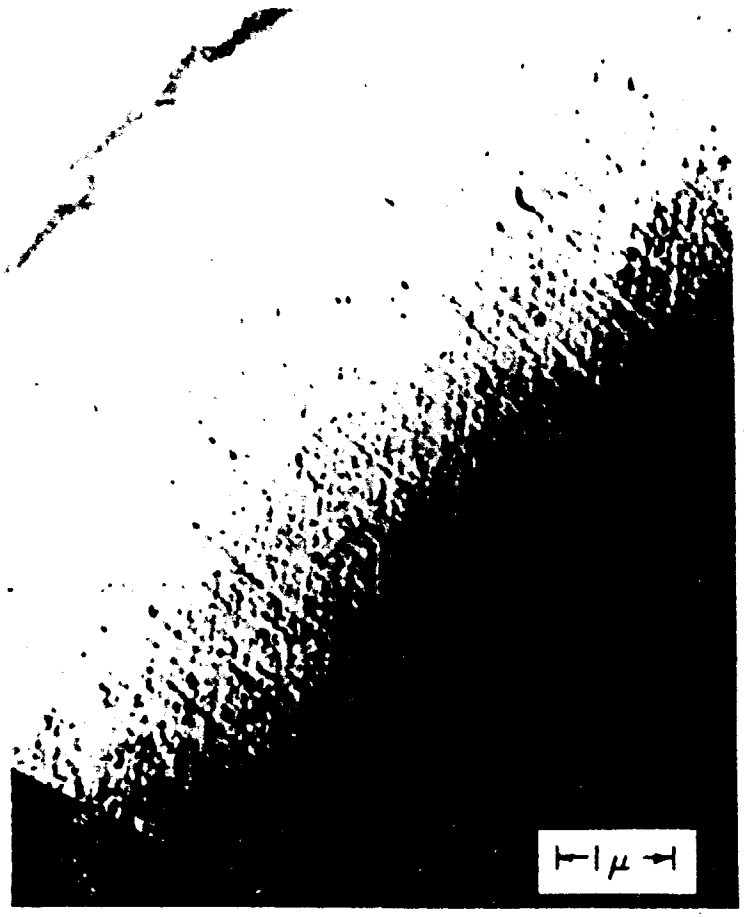


Fig. 7(b) - Near-Surface Transmission Electron Micrograph of Sample Shown in Fig. 1 (Not the Same Area), Showing Diffraction Contrast at Slip Lines. Operating Reflection is (200).

(a) Natural Oxide Layer

| 100 Å |

(b) 100 Å Oxide Layer

Fig. 8 - Aluminum Single Crystal Deformed at Atmospheric Pressure for 5,000 Cycles at $6 \times 10^{-4}$ Strain

(a) Natural Oxide Layer

| 100μ |

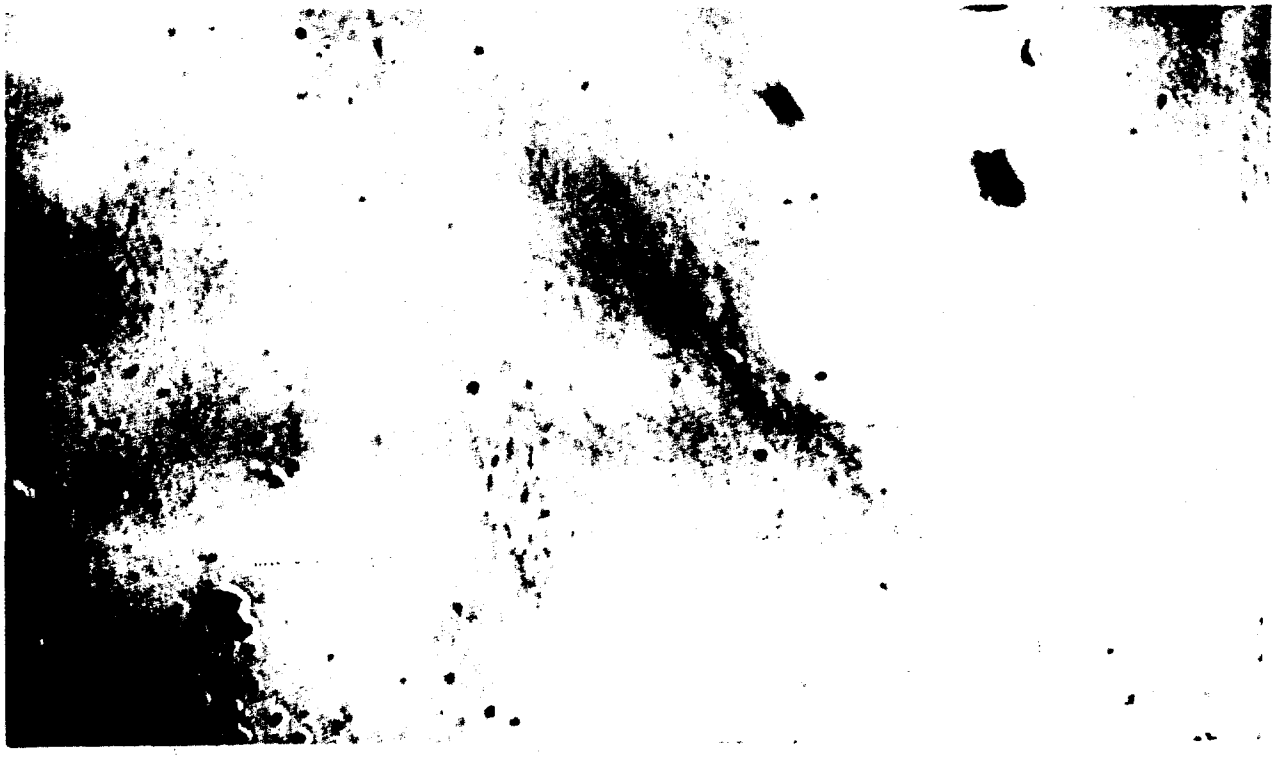

(b) 100 Å Oxide Layer

Fig. 9 - Aluminum Single Crystal Deformed at $1.3 \times 10^{-9}$ Torr for 5,000 Cycles at $6 \times 10^{-4}$ Strain

(a) Natural Oxide Surface

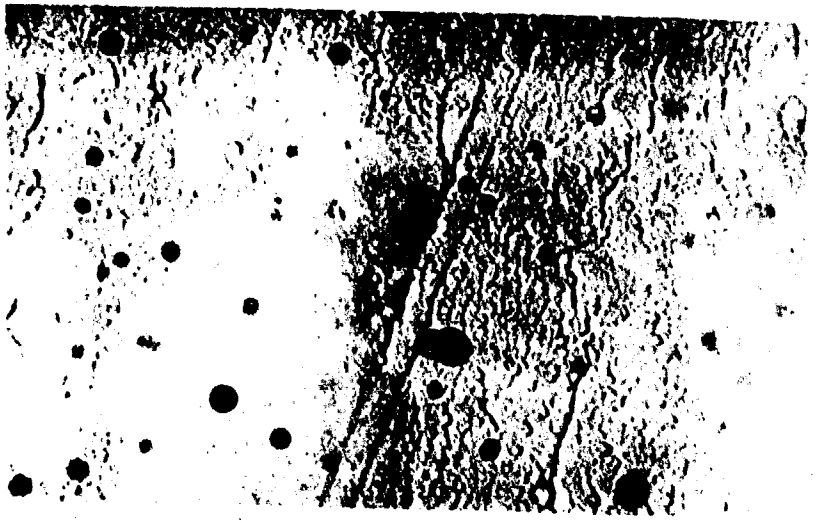

(b) 100 Å Oxide Surface



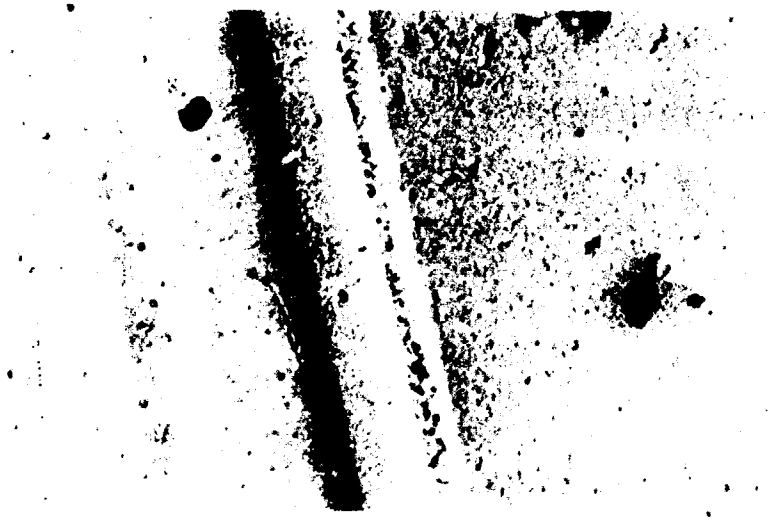

(c) 300 Å Oxide Surface

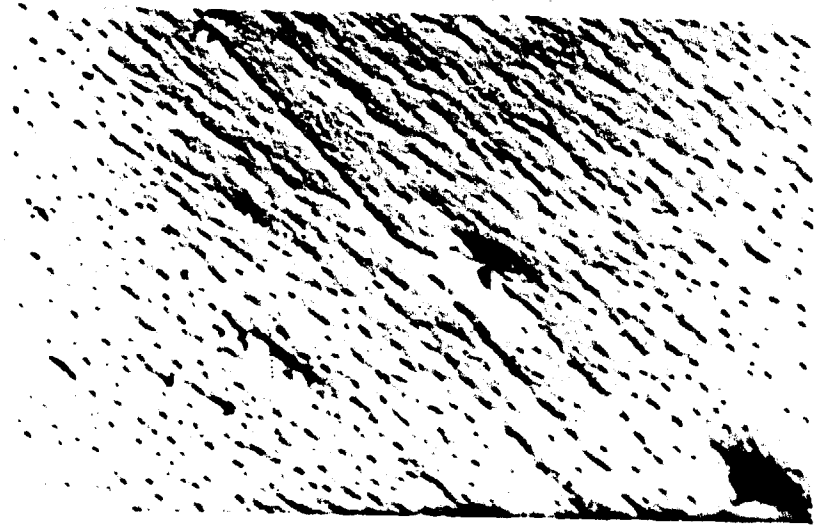

(d) 1,000 Å Oxide Surface

Fig. 10 - Electron Micrographs of Formvar Surface Replicas of the Aluminum Single Crystal Deformed at 760 Torr for 5,000 Cycles at $6 \times 10^{-4}$ Strain

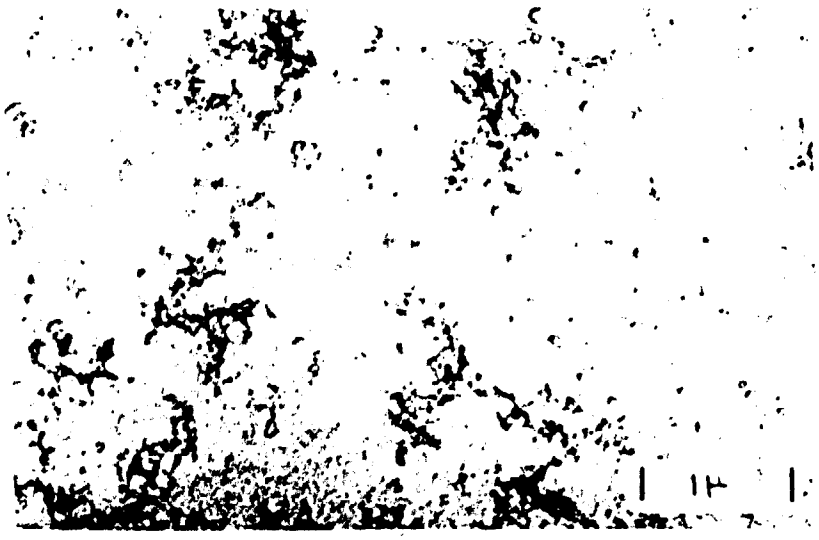

(b) Surface Beneath 300 Å Oxide Layer

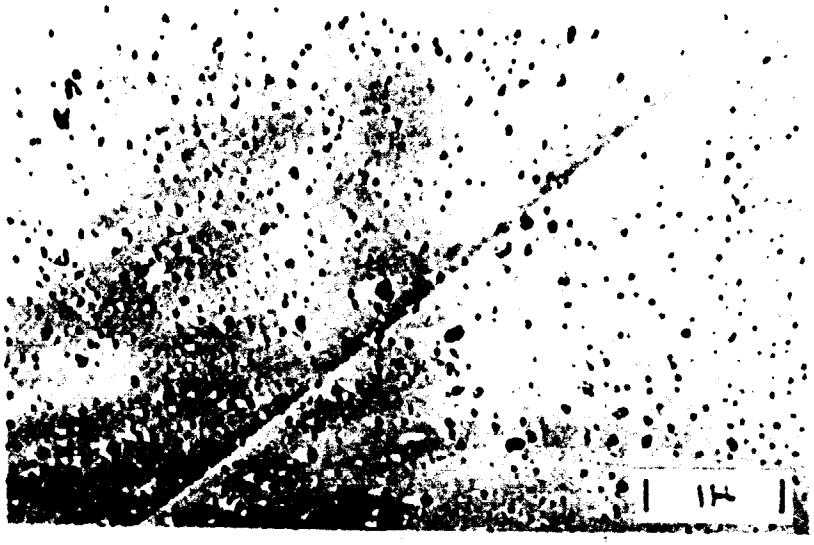

(a) Surface Beneath 100 Å Oxide Layer



(c) Surface Beneath 1,000 Å Oxide Layer

Fig. 11 - Electron Micrographs of Direct Replicas of the Metal Surface of the Aluminum Single Crystal Deformed 5,000 Cycles at 6 x $10^{-4}$ Strain at 760 Torr

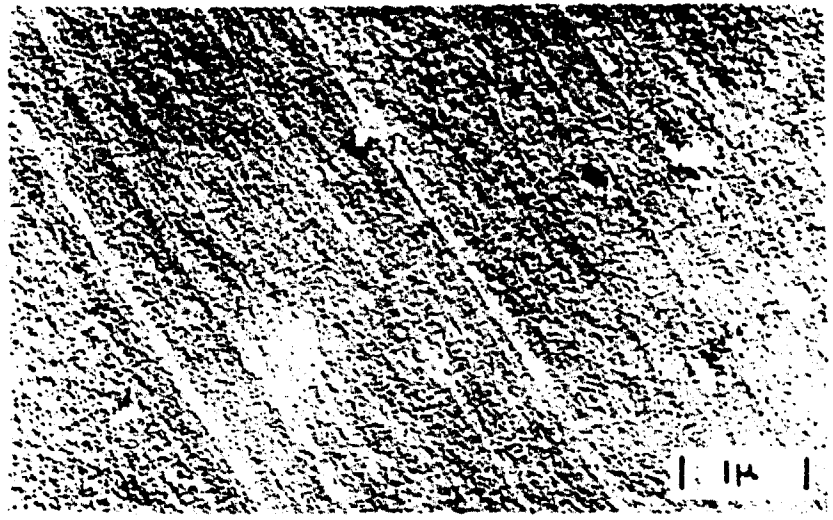

(a) Natural Oxide Layer

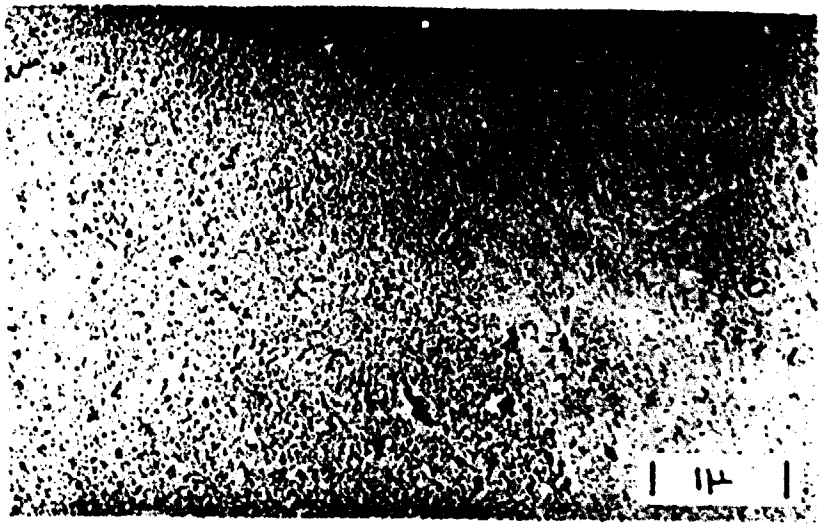

(b) 100 Å Oxide Layer



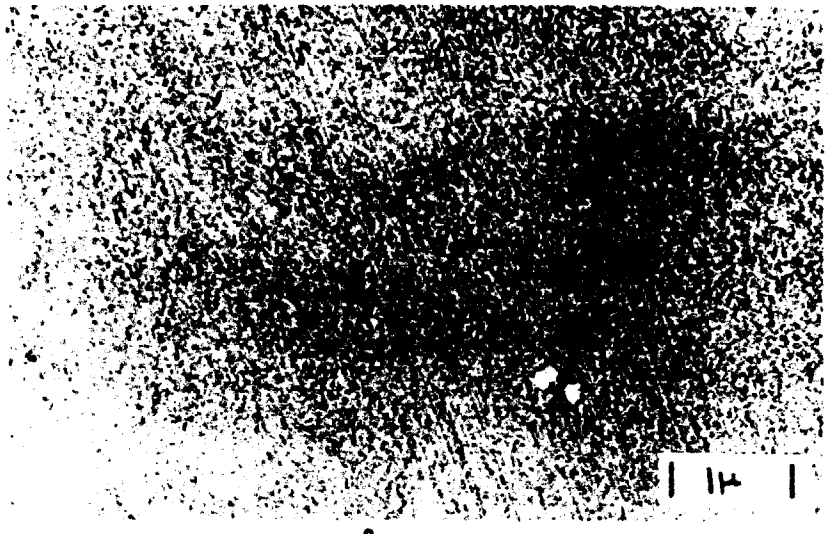

(c) 100 Å Oxide Layer

Fig. 12 - Electron Micrographs of Formvar Surface Replicas of Aluminum Single Crystal Deformed 5,000 Cycles at $6 \times 10^{-4}$ Strain in $1.3 \times 10^{-9}$ Torr Vacuum

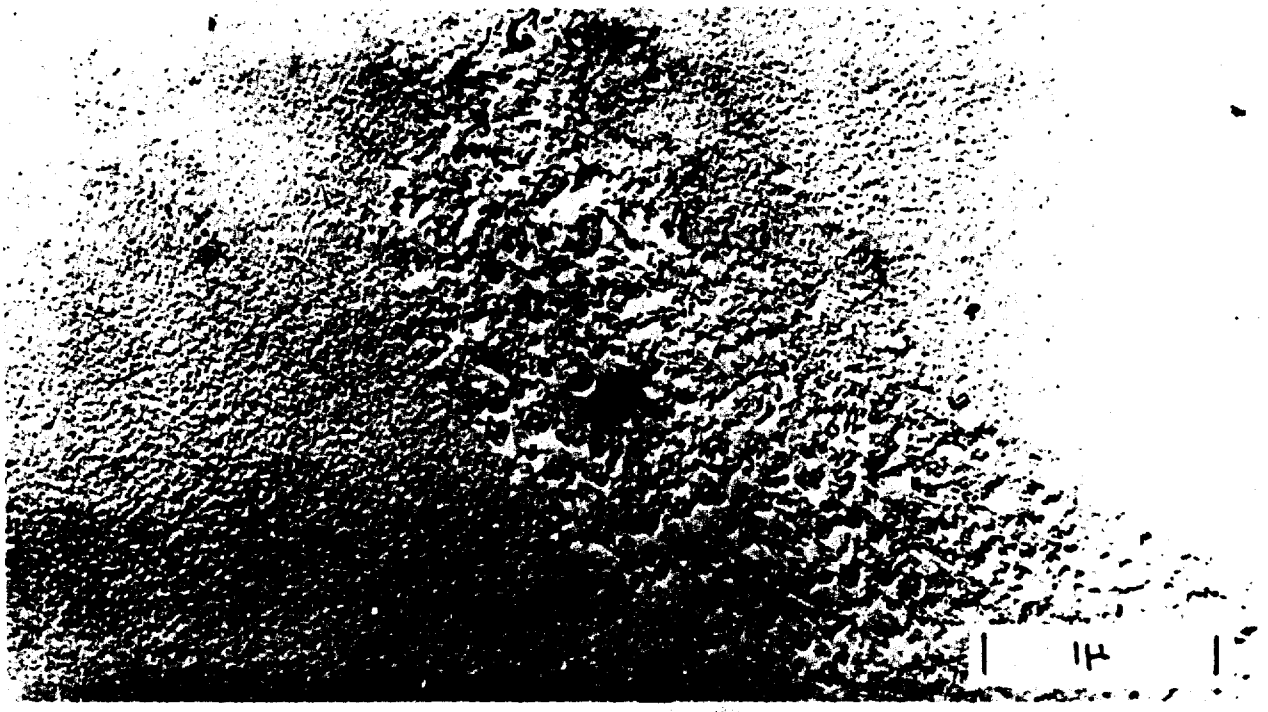


(a) 300 Å Oxide Layer

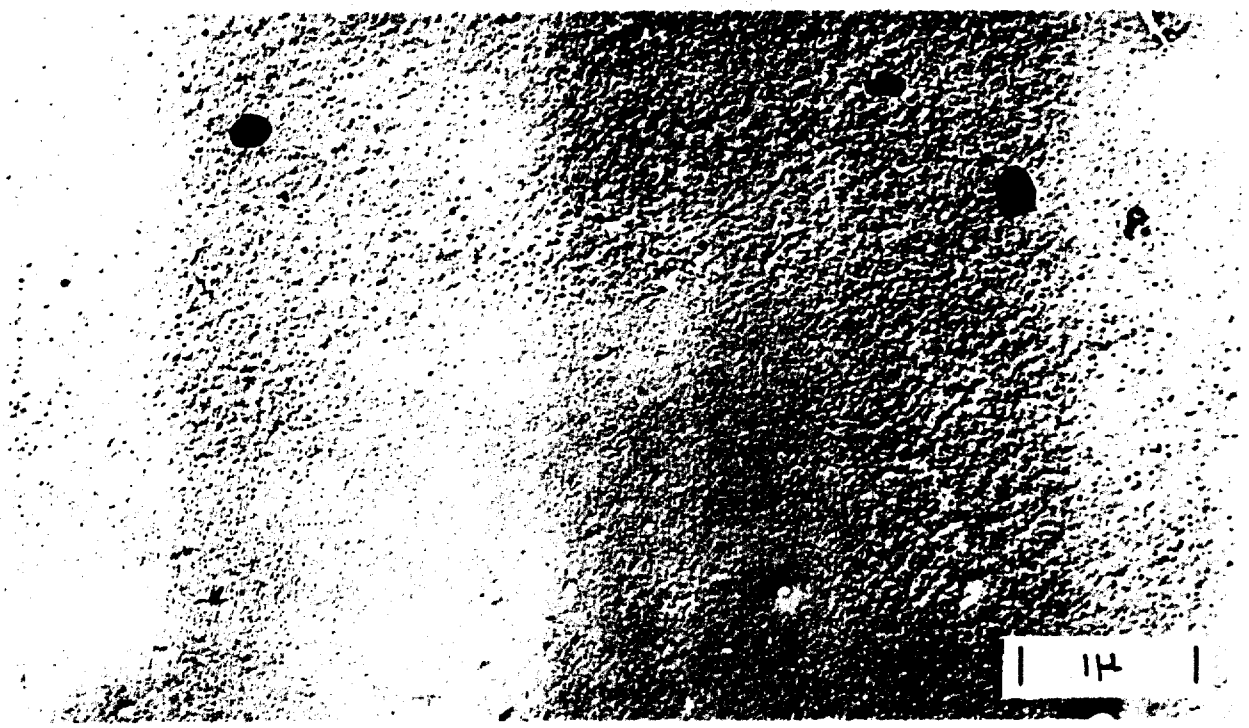


(b) 1,000 Å Oxide Layer

Fig. 13 - Electron Micrographs of Formvar Surface Replicas of the Aluminum Single Crystal Deformed 5,000 Cycles at $6 \times 10^{-4}$ Strain in $1.3 \times 10^{-9}$ Torr Vacuum

(a) Surface Beneath the 300 Å Oxide Layer

(b) Surface Beneath the 300 Å Oxide Layer

| 1μ |

(c) Surface Beneath the 1,000 Å Oxide Layer

Fig. 14 - Electron Micrographs of Direct Replicas of the Metal Surface of the Aluminum Single Crystal Deformed 5,000 Cycles at $6 \times 10^{-4}$ Strain in $1.3 \times 10^{-9}$ Torr Vacuum

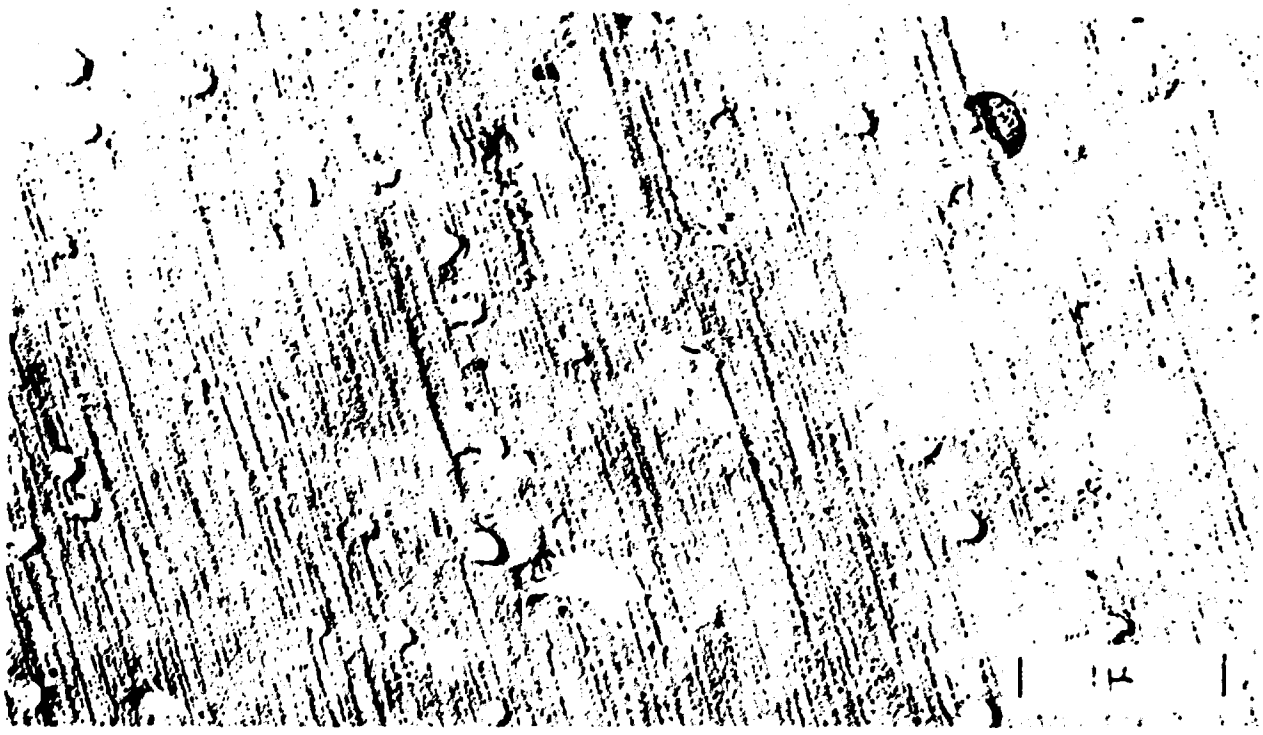

(a) Fine Dispersed Slip

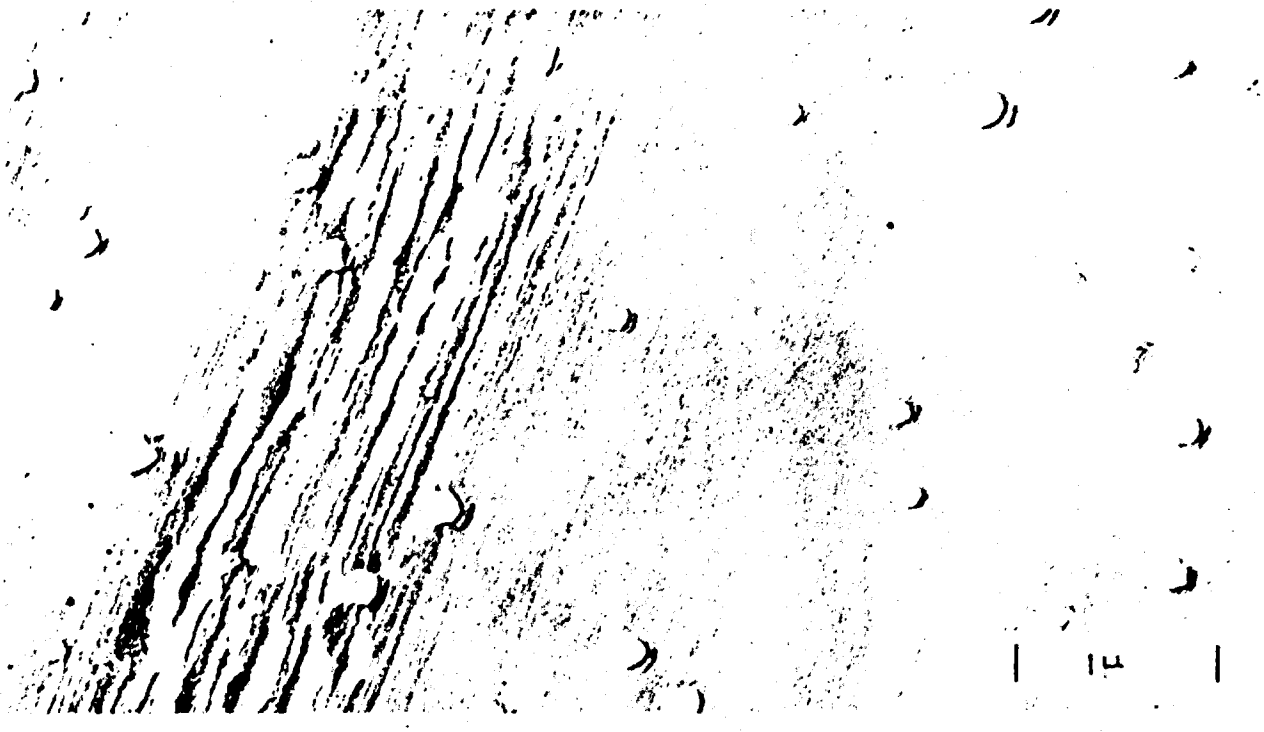

(b) Fine Dispersed Slip with Single Broad Band

Fig. 15 - Electron Micrographs of Surface Replicas of Polycrystalline Gold Deformed 10,000 Cycles at 2 x $10^{-3}$ Strain at 760 Torr


(a)

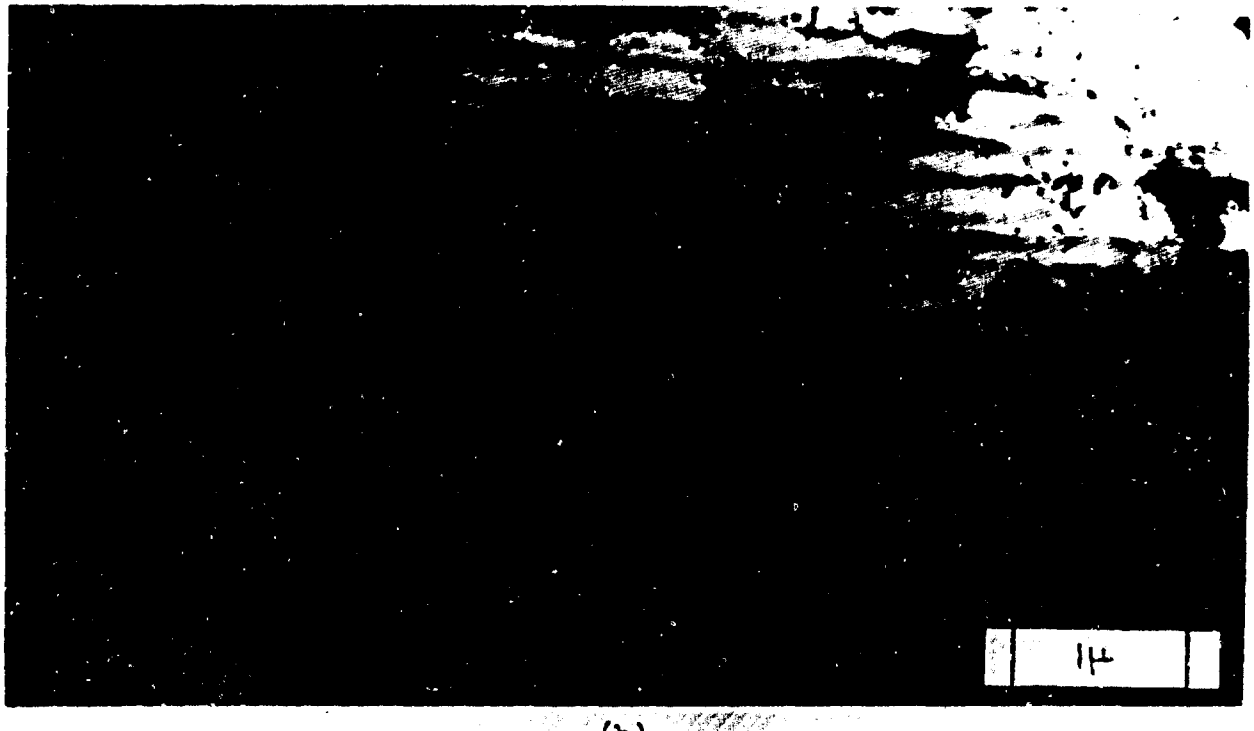


(b)

Fig. 16 - Near-Surface Transmission Micrograph of Polycrystalline Gold Deformed 10,000 Cycles at $2 \times 10^{-3}$ Strain in Air. Both (a) and (b) Show Slip Lines Visible by Diffraction Contrast.

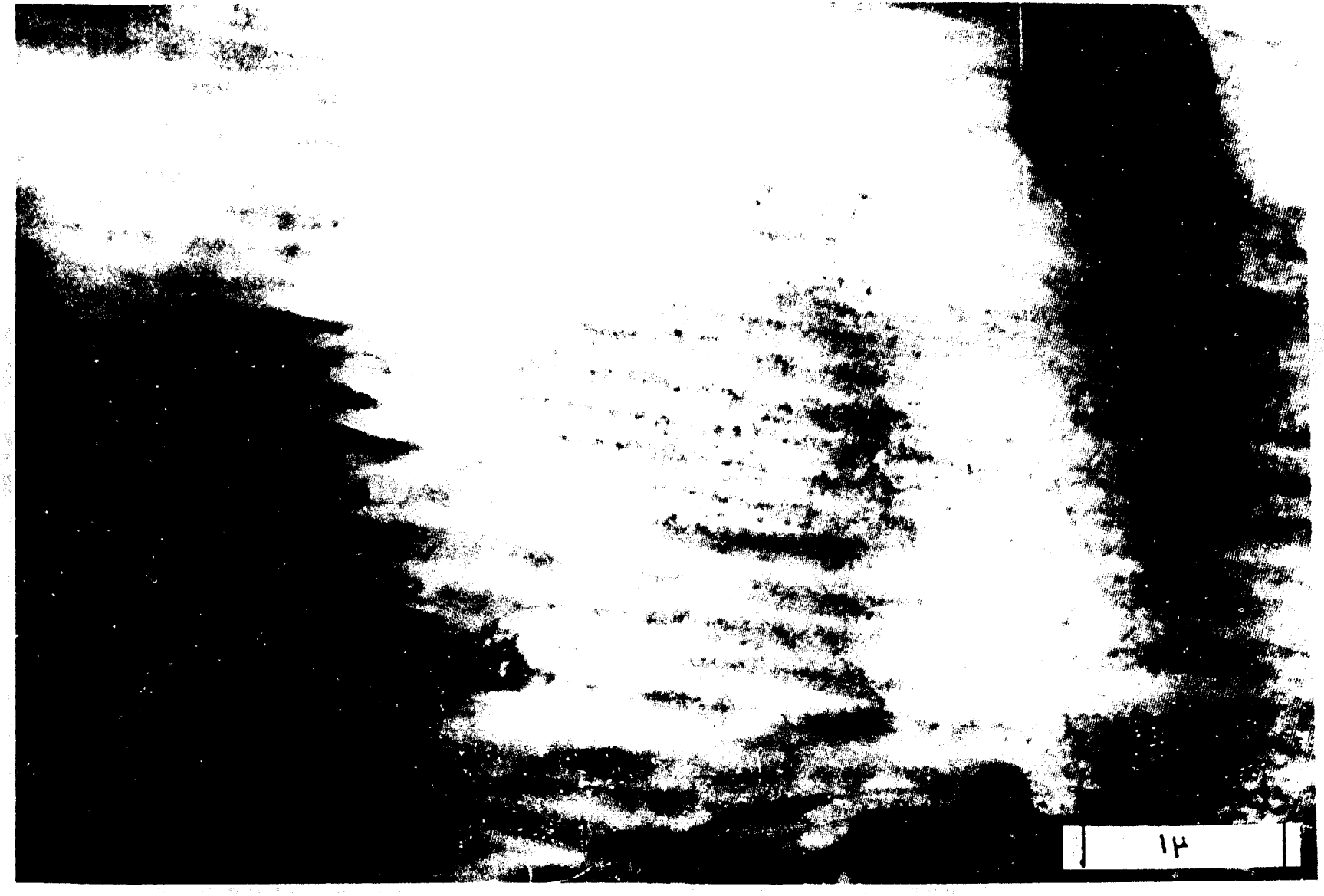


Fig. 17 - Near-Surface Transmission Micrograph of Gold Deformed 10,000 Cycles at $\pm$ 2 x $10^{-3}$ Strain in Air. Dislocation Loops Are Visible Lying Along the Slip Lines Which are Imaged by Thickness Contrast.

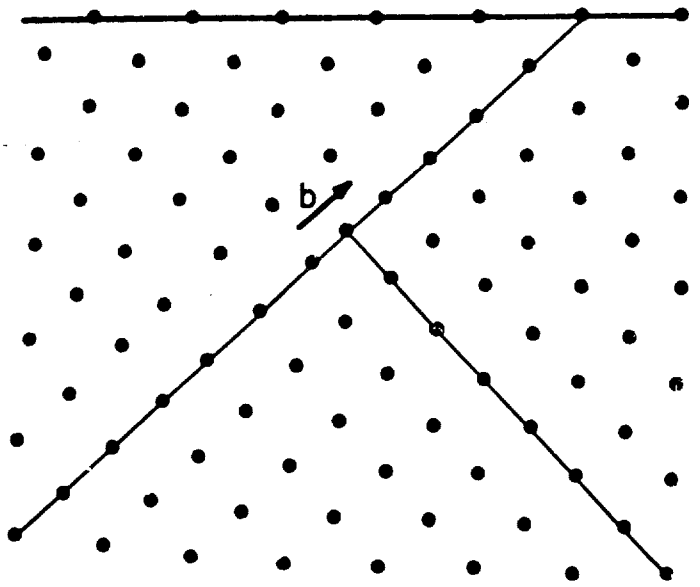


(a)

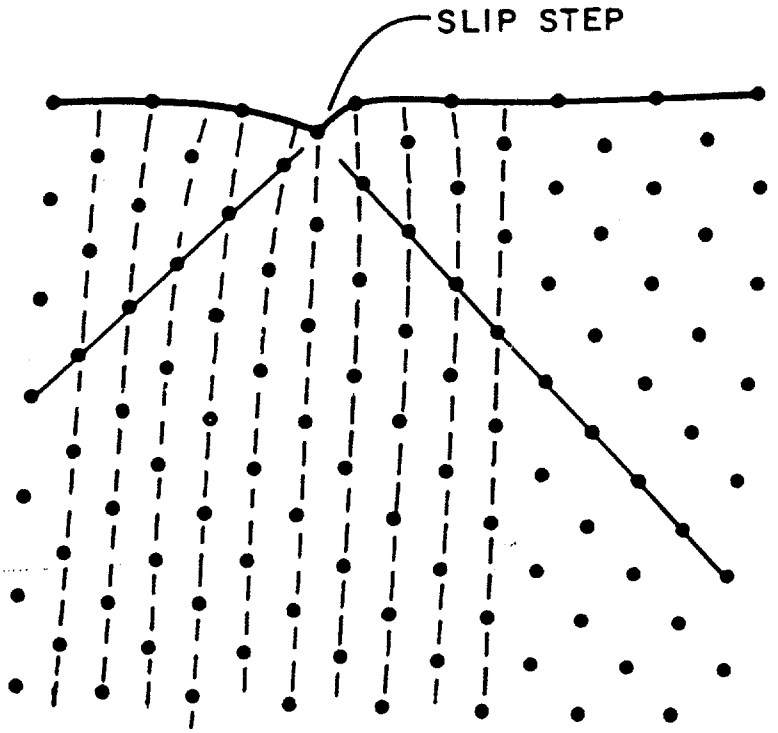


(b)

Fig. 18 - Proposed Model for Producing the Surface Strains Which Account for the Striations in Fig. 7. Near-Surface Edge Dislocation in (a) with Burger's Vector b Moves to Escape at Surface in (b) Producing Curvature in the Reflecting Planes (Dashed Lines).